Role of the N-Terminal Helix in the Metal Ion-Induced Activation of the Diphtheria Toxin Repressor DtxR

J. Alejandro D'Aquino,[‡] Judith R. Lattimer,[§] Andrew Denninger,[§] Katharine E. D'Aquino,[||] and Dagmar Ringe*[,‡,§]

Rosenstiel Basic Medical Sciences Research Center, Brandeis University, Waltham, Massachusetts 02454, Division of Endocrinology, Children's Hospital Boston, Harvard Medical School, Karp Family Research Laboratories, Room 4210, 300 Longwood Avenue, Boston, Massachusetts 02115, and Department of Biochemistry and Chemistry, Brandeis University, Waltham, Massachusetts 02454

Received April 26, 2007; Revised Manuscript Received July 31, 2007

ABSTRACT: The metal ion-regulated transcriptional repressor DtxR has been shown to repress the transcription of the diphtheria toxin and other genes associated with ferrous ion homeostasis in *Corynebacterium diphtheriae*. In vivo studies of single-alanine mutations located in the N-terminal helix of DtxR show that the activity of the mutants is reduced compared to that of the wild type. The three-dimensional structures of the apo and activated forms of DtxR show conformational changes in the N-terminal helix resulting from metal ion activation. We have studied the N-terminal helix mutants DtxR-(D6A,C102D), DtxR(E9A,C102D), and DtxR(M10A,C102D) using crystallographic and calorimetric techniques to gain insight into the possible reasons for such behavior at a molecular level. The binding affinities for metal ion extracted from the calorimetric titrations of the mutants DtxR(D6A,C102D) and DtxR(E9A,C102D) are very similar to those found for DtxR(C102D), while the same experiments performed with the mutant DtxR(M10A,C102D), bearing the M10A mutation located in binding site 2, show a decreased binding affinity in a predictable fashion. These results suggest that the decreased activity observed in these mutants cannot be explained exclusively by changes in the binding affinity of the repressor. The crystal structures of Ni-DtxR(M10A,C102D), Ni-DtxR(E9A,C102D), and Ni-DtxR(D6A,C102D) clearly show the presence of two metal ions bound. In the structure of Ni-DtxR(M10A,C102D), a water replaces Met10 in binding site 2. In the structure of Ni-DtxR(D6A,C102D), the nonhelical conformation of the N-terminal region characteristic of the activated form is absent. The side chain of Asp6 is critical in stabilization of the nonhelical conformation. This conformation is identical in all high-resolution structures of activated DtxR with an intact N-terminal helix, suggesting relevance in DtxR's regulatory function.

Ferrous ion is an essential nutrient of almost every organism. Bacteria depend on a limited environmental iron supply to cover their needs. To prevent deficiencies on the one hand and toxicity on the other, bacteria have evolved various mechanisms to achieve effective iron homeostasis. Pathogenic bacteria have linked the expression of virulence genes to the availability of ferrous ion. Once ferrous ion becomes growth-limiting, toxins and other virulence factors are expressed, resulting in the death of host cells, which makes their stored iron available to the bacteria. In *Corynebacterium diphtheriae*, the task of regulating the concentration of ferrous ion and the transcription of virulence factors is carried out by the diphtheria toxin repressor.

The diphtheria toxin repressor (DtxR)[1] is the best-characterized example of a widespread family of proteins found in many pathogenic bacteria, such as *Mycobacterium tuberculosis*, *Treponema pallidum*, and *Streptococcus pyogenes*, among others (*1*−*3*). Crystallographic studies of DtxR revealed two major structural domains linked by a flexible, proline-rich linker (*4*, *5*). These consist of an N-terminal domain that contains a helix−turn−helix (HTH) motif and a C-terminal domain that exhibits an SH3-like fold (*8*−*10*). However, not all members of the DtxR family have two domains: several members lack the C-terminal domain (*6*, *7*). The N-terminal domain of DtxR contains two metal ion binding sites (*4*, *5*, *8*). Binding site 1 consists of the side chains of His79, Glu83, and His98 from the N-terminal domain (*4*, *5*). Some structures of DtxR show that the side chains of two residues from the C-terminal domain, Glu170 and Gln173, may also contribute to binding site 1 (*9*). In some DtxR structures where no interaction is seen between residues from the C-terminal domain and binding site 1, an anion, usually a phosphate or sulfate ion, participates as a ligand (*10*, *11*). Binding site 2 consists of the side chains of Glu105, His106, Cys102, Met10, the carbonyl oxygen of

* To whom correspondence should be addressed: Rosenstiel Basic Medical Sciences Research Center MS029, Brandeis University, Waltham, MA 02454. Phone: (781) 736-4902. Fax: (781) 736-2405. E-mail: ringe@brandeis.edu.

[‡] Rosenstiel Basic Medical Sciences Research Center, Brandeis University.

[§] Department of Biochemistry and Chemistry, Brandeis University.

[||] Harvard Medical School.

[1] Abbreviations: DtxR, diphtheria toxin repressor; HTH, helix−turn−helix; SH3, Src homology 3 domain; ITC, isothermal titration calorimetry; IPTG, isopropyl thiogalactoside; SDS−PAGE, sodium dodecyl sulfate−polyacrylamide gel electrophoresis; PEG, poly(ethylene glycol); Ni−NTA, nickel−nitrilotriacetic acid; DEAE, diethylaminoethyl; OD, optical density.

10.1021/bi7007883 CCC: $37.00
Published on Web 09/29/2007

Cys102, and a water molecule (*5*, *12*). Mutational studies have shown that the integrity of both binding sites is essential for repressor activity (*13*). While in vivo the metal ion-induced activation of DtxR is specific for Fe(II), the activation in vitro of DtxR is not metal ion-specific, and several divalent transition metal ions have been shown to activate the repressor in addition to ferrous ion in the following order of activation: Fe(II) ∼ Ni(II) > $Co(II)^+$ ≫ Mn(II) (*14*, *15*). In the presence of ferrous ion, DtxR forms a homodimer that binds to the *tox* operator, preventing downstream transcription of genes, including the virulence genes. Below a certain concentration of ferrous ion, this DtxR−*tox* operator complex dissociates and transcription occurs.

Because of the importance of the metal ion-induced activation of DtxR in repression of virulence factors, there has been a great deal of interest in the elucidation of the events that lead to an active repressor at a molecular level. We have recently demonstrated that DtxR has a high-affinity binding site and a low-affinity binding site corresponding to binding sites 1 and 2, respectively (*16*). Spectroscopic measurements performed on MntR, a DtxR homologue from *Bacillus subtilis*, give similar results (*17*). Using a combination of calorimetric and crystallographic techniques, we have proposed a mechanism for the metal ion-induced activation of DtxR, which can be summarized as follows (*16*). In the absence of divalent transition metal ions, DtxR exists primarily as a monomer. As the concentration of the metal ion increases, coordination to binding site 1 occurs with no noticeable conformational changes. Once binding site 1 is saturated, coordination of metal ion to binding site 2 follows, accompanied by a small but noticeable conformational change in the N-terminal helix, where the first six residues undergo a conformational change often termed a helix-to-coil transition (*16*). It was inferred that binding site 2 serves as a metal ion sensor and determines the metal ion concentration at which the repressor can be active, while binding site 1 contributes to the stability and persistence of the tertiary structure of the protein by anchoring key residues and extending the lifetime of the interactions of an extensive electrostatic network (*5*, *9*, *11*, *13*). Although our experiments do not determine when dimerization takes place during activation, it would seem reasonable that it occurs as a result of the observed conformational changes. Because the three-dimensional structure of activated DtxR does not seem to be affected significantly by the presence or absence of DNA, it is believed that the DNA does not actively participate in the process of metal ion-induced activation (*5*, *18*). A recent report presenting a complex of IdeR from *M. tuberculosis* with its operator DNA opens the possibility that the activated form of DtxR-like repressors must be optimized for DNA binding (*19*). This study, however, leaves open the question of whether it is the conformation of the protein or the operator DNA that has to be optimized (*19*).

One aspect of the metal ion-induced activation of DtxR that remains unknown deals with the signal transduction that operates between metal ion coordination and the observed conformational changes during the activation process. For instance, it is known that the N-terminal helix is highly conserved among members of the DtxR family. This conservation at the primary sequence level could be indicative of a prominent role of the N-terminal helix in the function of the repressor. In fact, single-alanine replacements of some of the N-terminal helix residues lead to reduced activity. In vivo, the mutants DtxR(D6A) and DtxR(E9A) show a decrease in activity of 20−40% when compared to the wild type, and the mutant DtxR(M10A) is completely inactive. In the case of the latter, Met10 participates as a ligand of binding site 2; thus, a change in binding affinity for metal ion could also be anticipated. In fact, reconstitution experiments show a decrease in the amount of total metal ion coordinated when compared to that with the wild type (*14*). These considerations motivated us to study the N-terminal helix of DtxR and its possible role in activation of the repressor.

We have purified the N-terminal helix mutants DtxR-(D6A,C102D), DtxR(E9A,C102D), and DtxR(M10A,C102D), determined their crystal structures, and determined their binding affinities for Ni(II) ion calorimetrically to study the role of the N-terminal helix in the metal ion activation of DtxR. Mutagenesis studies have shown that the only amino acid that can be substituted for Cys102 while preserving repressor activity is Asp (*8*). The C102D mutation was thus employed in crystallographic studies to prevent oxidation of sulfur from influencing the structure around binding site 2 (*8*, *16*, *20*, *21*).

EXPERIMENTAL PROCEDURES

Cloning and Protein Expression. DtxR mutants were subcloned from pET-11c-*dtxr* using the QuikChange mutagenesis kit (Stratagene, La Jolla, CA). Mutagenic oligonucleotide primers were synthesized by Qiagen (Valencia, CA). DtxR(C102D) was subcloned first and subsequently used for cloning DtxR(M10A,C102D), DtxR(E9A,C102D), and DtxR(D6A,C102D). These resulting plasmids were sequenced to verify that the proper mutants were obtained (Seqwright, Houston, TX). Protein expression was induced by isopropyl thiogalactoside (IPTG) (final concentration of 0.5 mM) at an OD of 0.6 after transformation of the plasmid DNA containing DtxR(M10A,C102D), DtxR(E9A,C102D), and DtxR(D6A,C102D) sequences into BL21(DE3) cells at 37 °C. After induction, the cells were left in the incubator for an additional 2 h. Following that, the cells were harvested by centrifugation, frozen, and stored at −80 °C until further use.

Purification of DtxR Mutants. The previously described purification protocol was used with slight modifications (*16*). The cell pellet was thawed and resuspended in 50 mL of 10 mM Tris-HCl (pH 7.5) and then lysed by sonication. The lysate was centrifuged at 13000*g* for 45 min at 4 °C. The supernatant was loaded first onto a DEAE (diethylaminoethyl) Cephacel (Sigma-Aldrich, St. Louis, MO) anion exchange column equilibrated with 10 mM Tris-HCl (pH 7.5) and washed with 200 mL of 10 mM Tris-HCl (pH 7.5). Protein was eluted with a 300 mL linear gradient from 0 to 300 mM NaCl at a flow rate of 1 mL/min. DtxR(D6A,-C102D), DtxR(E9A,C102D), and DtxR(M10A,C102D) eluted at approximately 220−300 mM NaCl as determined by SDS−PAGE. Fractions containing DtxR mutants were pooled, concentrated, loaded onto a nickel−nitrilotriacetic acid (Ni−NTA) affinity column (Qiagen) pre-equilibrated with 10 mM Tris-HCl (pH 7.5), and then washed with 100 mL of 10 mM Tris-HCl (pH 7.5). Protein was eluted with a

Table 1: Data Collection and Refinement Statistics

	Ni-DtxR(D6A,C102D) (PDB entry 2QQ9)	Ni-DtxR(E9A,C102D) (PDB entry 2QQA)	Ni-DtxR(M10A,C102D) (PDB entry 2QQB)
	Data Collection		
temperature (K)	100	100	100
space group	$P3_121$	$P3_121$	$P3_121$
$a = b$; c (Å)	62.71; 107.4	61.76; 104.6	62.32; 104.6
$\alpha = \beta$; γ	90; 120	90; 120	90; 120
resolution range (Å)	27−1.7	35−2.1	30−1.9
no. of observed reflections	107865	247163	114192
no. of unique reflections	21573	13090	15860
signal to noise $\langle I/\sigma(I)\rangle$	4.9	12.0	6.0
completeness of data (%)/[last shell[a] (%)]	84/(48)	98/(97)	90/(42)
redundnacy	5.0	17.9	7.2
R_{merge}[b] (%)/[last shell[a] (%)]	13.5/(79)	8.7/(60)	11.4/(60)
	Refinement		
no. of reflections used [working/(free)]	21573/(1152)	13090/(686)	15860/(853)
R_{factor}[c] (%)	24	20	22
R_{free} (%)	29	26	31
total no. of non-hydrogen atoms	1901	1810	1807
no. of Ni(II) ions	2	2	2
rms deviation			
bond lengths (Å)	0.02	0.03	0.03
bond angles (deg)	1.8	2.3	2.5
mean *B*-factor	20	32	24

[a] Highest-resolution shell for mutants: DtxR(D6A,C102D), 1.7−1.8 Å; DtxR(E9A,C102D), 2.1−2.2 Å; and DtxR(M10A,C102D), 1.9−2.0 Å. [b] $R_{merge} = (\sum|I_{obs} - I_{ave}|)/(\sum I_{ave})$, over all symmetry-related observations. [c] $(\sum|F_o - F_c|)/(\sum F_o)$, over all reflections.

100 mL linear gradient from 0 to 10 mM imidazole in the same buffer at a flow rate of 2 mL/min. Fractions containing the protein of interest were identified by SDS−PAGE, pooled, concentrated to 15 mg/mL, and stored at −80 °C until they were used.

Protein Crystallization. Samples of DtxR(D6A,C102D), DtxR(E9A,C102D), and DtxR(M10A,C102D) were kept in 10 mM Tris-HCl (pH 7.5) at a concentration of 7.5 mg/mL and crystallized by vapor diffusion using the hanging drop method at room temperature. The protein solution (5 μL) was mixed with an equal amount of well solution [0.2 M Na_2HPO_4, 20% poly(ethylene glycol) (PEG) 3350, and 5 mM $NiCl_2$]. Crystals suitable for X-ray diffraction appeared within 1 week. Prior to crystallographic experiments, samples were incubated in a cryoprotecting solution containing 30% PEG 400 for 30 s.

Data Collection. Diffraction data for Ni-DtxR(D6A,-C102D) and Ni-DtxR(M10A,C102D) were collected in house on an Xcalibur PX Ultra diffractometer system equipped with an Onyx CCD detector (Oxford Diffraction, Oxfordshire, U.K.) at 100 K to a resolution of 1.71 Å for Ni-DtxR(D6A,-C102D) and 1.92 Å for Ni-DtxR(M10A,C102D). The data were integrated and indexed using MOSFLM and scaled using SCALA from the CCP4 suite (*22*, *23*). The data for Ni-DtxR(E9A,C102D) were collected to 2.10 Å at beamline 23-ID of the Advanced Photon Source at Argonne National Laboratory (Argonne, IL). Diffraction data were collected at 100 K on a MARmosaic 300 CCD detector (Mar USA, Evanston, IL) and processed with HKL2000 (*24*).

Structure Determination and Refinement. The structures of Ni-DtxR(D6A,C102D), Ni-DtxR(M10A,C102D), and Ni-DtxR(E9A,C102D) were determined by molecular replacement using the program PHASER of the CCP4 suite, using DtxR(H79A) (PDB entry 1P92) as a search model (*18*−*20*). The crystals have the symmetry of space group $P3_121$ with one molecule per asymmetric unit. After a round of rigid body refinement and several rounds of manual positioning and restrained refinement using Coot for molecular display and REFMAC5, the refinement proceeded until the R_{free} could no longer be reduced (*22*, *25*). During refinement, two Ni(II) ions and a phosphate anion were included in the structure, resulting in a significant reduction in R_{factor} and R_{free}. Complete statistics for the refinement are presented in Table 1. Refinement of Ni-DtxR(D6A,C102D) and Ni-DtxR-(M10A,C102D) produced a gap between R_{factor} and R_{free} slightly greater than expected. This fact has been attributed to an unusually large number of rejected reflections due to spot overlap.

Isothermal Titration Calorimetry. ITC experiments were performed using a VP-ITC microcalorimeter (Microcal Inc., Northampton, MA) at 25 °C. Metal ion free samples and buffers were obtained using the method proposed by Spiering et al. (*14*) using Chelex resin (Bio-Rad Laboratories, Hercules, CA) as a chelating agent. Metal ion free protein samples were dialyzed against 0.1 M Tris-HCl (pH 7.5) and degassed prior to the experiments. Protein samples at a concentration of 20−60 μM were titrated against 0.1 M Tris buffer (pH 7.5) containing $NiCl_2$ in the concentration range of 1−5 mM. The higher limit of metal ion concentration was used in an attempt to resolve poor signal to noise in the region of complete saturation observed in the titration of DtxR(M10A,C102D). The data were fitted by using Microcal ORIGIN supplied with the instrument. The data were best fitted to a two-binding site model. Binding affinities were calculated using a 1 M standard state.

RESULTS

Overall Structure. The overall conformations of the Ni-DtxR(D6A,C102D), Ni-DtxR(M10A,C102D), and Ni-DtxR-(E9A,C102D) structures correspond to the previously described pattern of secondary structure motifs (*4*, *5*, *11*). The N-terminal domain contains six α-helices, designated by the letters A−F, and two β-strands. The two metal ion binding

FIGURE 1: Monomer of Ni-DtxR(D6A,C102D) showing the relative positions of the N-terminal and C-terminal domains. The N-terminal domain is colored blue, except for the HTH motif (magenta), the N-terminal helix with the D6A, E9A, and M10A mutations shown in ball and stick (green), and two metal ions (gray). The C-terminal domain is colored red. The sulfate ion is colored purple. All figures were generated by using MOLSCRIPT and POVSCRIPT+ (*40*, *41*).

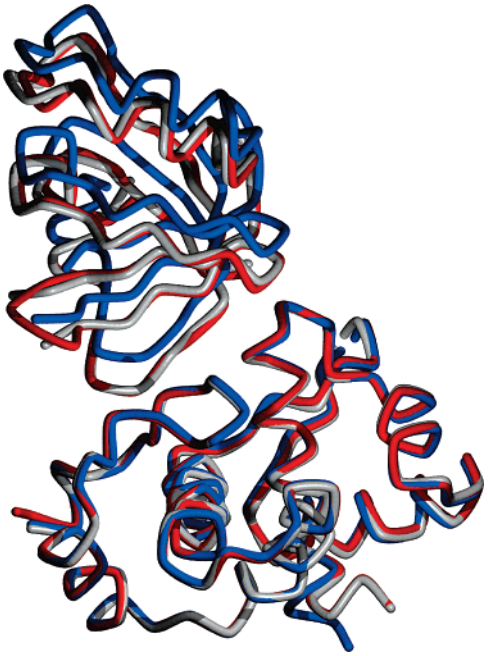

FIGURE 2: Overlay of the structures of Ni-DtxR(D6A,C102D), Ni-DtxR(E9A,C102D), and Ni-DtxR(M10A,C102D). When the N-terminal domains of these mutants are aligned, their C-terminal domains do not superimpose well. The relative positions of the N-terminal and C-terminal domains observed in Ni-DtxR(D6A,-C102D) (blue), Ni-DtxR(E9A,C102D) (red), and Ni-DtxR(M10A,-C102D) (gray) show rms displacements of approximately 1.4 Å.

sites and the helix−turn−helix motif that is involved in DNA recognition are found in the N-terminal domain. The Cα atoms of the N-terminal domain residues (6−139) of the three structures can be superimposed with a root-mean-square (rms) deviation of <0.3 Å. The C-terminal domain contains five β-strands that form a conformation similar to that found in the SH3 fold (*11*, *26*). The monomer of Ni-DtxR(D6A,-C102D), indicating the relative positions of the two metal ion binding sites, the position of the HTH motif, and the position of the D6A, E9A, and M10A mutations in the N-terminal helix, is shown in Figure 1. The HTH motifs of all the mutants studied here have conformations identical to that of the DtxR−DNA complex. No interactions between residues from the C-terminal domain and binding site 1 or their corresponding symmetry-related pairs are observed in the crystal structures presented here. When the N-terminal domains (residues 6−139) of Ni-DtxR(D6A,C102D), Ni-DtxR(M10A,C102D), and Ni-DtxR(E9A,C102D) are superimposed, the C-terminal domain residues (150−226) of these mutants do not superimpose well. The rms displacement for the alignment of the C-terminal domain with respect to the N-terminal domain is 1.39 Å between Ni-DtxR(E9A,C102D) and Ni-DtxR(D6A,C102D) and 1.35 Å between Ni-DtxR-(M10A,C102D) and Ni-DtxR(D6A,C102D) (see Figure 2). No model was built for the region corresponding to the linker that connects the N-terminal and C-terminal domains (residues 140−149). This linker is flexible and therefore refractory to crystallographic analysis.

The structure of Ni-DtxR(D6A,C102D) contains the N-terminal domain, residues 3−139, and the C-terminal domain, residues 150−198 and 201−226. The electron density is continuous throughout the main chain of the visible part of the sequence with electron density for only a few side chains missing. The structure was refined with all modeled residues in allowed regions of the Ramachandran plot. Similarly, the structure of Ni-DtxR(E9A,C102D) contains the N-terminal domain, residues 3−140, and a complete C-terminal domain, residues 147−226, with the exception of a few side chains. The electron density is continuous for the visible regions, and the geometry of the refined structure is good. Finally, the structure of Ni-DtxR(M10A,C102D) contains the N-terminal domain, residues 3−139, and the C-terminal domain, residues 149−198 and 200−226. The electron density is continuous covering the whole range of visible residues. Only a few side chains are missing from the modeled regions. Only four non-glycine residues occupy traditionally nonallowed regions of the Ramachandran plot, among them, Val5. This is consistent with previously published structures of DtxR (*20*, *27*).

Metal Ion Binding Sites. Each of the three structures reported in this article contains two fully occupied metal ion binding sites. The occupancy of the metal ion [Ni(II)] was demonstrated by the presence of strong peaks in the difference ($F_o - F_c$) electron density map at a high sigma level ($\sigma > 10$) after the protein model had been built. A complete list of the metal ion−ligand distances for the three structures is given in Tables 2 and 3.

Binding Site 1. In the three structures reported in this article, binding site 1 is located between α-helices E and F and consists of the side chains of residues His79, Glu83, and His98, a phosphate ion, and at least one water molecule (see Figure 3). Coordination of the anion in these structures is consistent with previously published DtxR structures that have shown a phosphate or sulfate anion acting as a ligand

Table 2: Metal Ion−Ligand Distances in Binding Site 1 in Angstroms

ligand or protein	DtxR(D6A, C102D)	DtxR(E9A, C102D)	DtxR(M10A, C102D)
Glu83 Oϵ2	2.2	2.1	2.4
His79 Nϵ2	2.2	2.2	2.1
His98 Nδ1	2.2	2.3	2.4
PO_4	2.2	2.2	2.3
water 1	2.2	2.2	–
water 2	2.2	2.3	2.4

Table 3: Metal Ion−Ligand Distances in Binding Site 2 in Angstroms

ligand or protein	DtxR(D6A, C102D)	DtxR(E9A, C102D)	DtxR(M10A, C102D)
Met10 Sδ	2.4	2.6	2.5 (water)
Asp102 O	2.1	2.1	2.3
Asp102 Oδ1	2.2	2.3	2.4
Glu105 Oϵ2	2.1	2.3	2.4
His106 Nϵ2	2.2	2.3	2.1
water	2.3	2.2	2.2

in binding site 1 (*4*, *18*). Interestingly enough, although several other DtxR structures show contributions from residues Glu170 and Gln173 located in the C-terminal domain to binding site 1, these interactions are not present in any of these structures (*9*).

The Ni(II) ions in binding site 1 of Ni-DtxR(D6A,C102D) and Ni-DtxR(E9A,C102D) display octahedral geometry. To the best of our knowledge, this is the first time that the metal ion is seen crystallographically with such a geometry at binding site 1. All previously reported crystal structures for DtxR and mutants show coordination of either four or five ligands at this site (*4*, *5*, *9*, *26*). Structures of the structural and functional DtxR homologue, IdeR, have also shown the pentavalent coordination pattern at binding site 1 (*19*, *28*, *29*). The calculated *B*-factors for the Ni(II) ion of Ni-DtxR-(D6A,C102D) and Ni-DtxR(E9A,C102D) are 25 and 24 Å^2, respectively. In contrast to the structures of Ni-DtxR(D6A,-C102D) and Ni-DtxR(E9A,C102D), the structure of Ni-DtxR(M10A,C102D) shows a pentavalently coordinated Ni(II) ion binding to binding site 1, with a single water molecule completing the distorted trigonal bipyramidal geometry. The calculated *B*-factor for the Ni(II) ion in binding site 1 of this structure is 21 Å^2. The water molecules that complete coordination at binding site 1 of Ni-DtxR-(M10A,C102D) superimpose well with one of the two water molecules found in both DtxR(D6A,C102D) and Ni-DtxR-(E9A,C102D).

Binding Site 2. Binding site 2 of the three structures reported is located between α-helices A and E, and the Ni-(II) ion at this site displays octahedral geometry. In all the structures, the side chains of Asp102, Glu105, and His106, the carbonyl oxygen of Asp102, and at least one water molecule participate as ligands. In the structures of both Ni-DtxR(E9A,C102D) and Ni-DtxR(D6A,C102D), Sδ of Met10 completes the coordination environment of the metal ion (see Figure 4). In the structure of Ni-DtxR(M10A,C102D), a water molecule replaces Met10 as the ligand, occupying the same position as Sδ of Met10. The C102D mutation allows metal ion binding at site 2 and contributes to its high occupancy by removing the possibility of oxidation of Cys102, which often interferes with metal ion binding (*4*, *10*, *11*, *16*). Coordination at this site is consistent with previously published crystal structures of wild-type DtxR and variants bearing the C102D mutation (*8*, *16*, *20*, *21*). The calculated *B*-factors for the Ni(II) ion at binding site 2 are 25, 36, and 25 Å^2 for Ni-DtxR(D6A,C102D), Ni-DtxR(E9A,-C102D), and Ni-DtxR(M10A,C102D), respectively.

N-Terminal Helix. The overall conformational changes of the N-terminal helices of Ni-DtxR(D6A,C102D), Ni-DtxR-(E9A,C102D), and Ni-DtxR(M10A,C102D) are presented in Figure 5. The electron densities for Ni-DtxR(D6A,C102D), Ni-DtxR(E9A,C102D), and Ni-DtxR(M10A,C102D) are very weak for the first two residues, indicating a high degree of flexibility, which prevented model building. Starting at Asp3, the structure of Ni-DtxR(D6A,C102D) is helical until residue Glu21, where a turn starts. The typical hydrogen bonding pattern of α-helices is found throughout this region of the structure. In the structures of Ni-DtxR(E9A,C102D) and Ni-DtxR(M10A,C102D), the first three residues adopt a non-helical conformation and the helical hydrogen bonding pattern does not commence until residue Thr7. The conformation of the first three visible residues of Ni-DtxR(E9A,-C102D) and Ni-DtxR(M10A,C102D) can be superimposed on that found in previously published structures of active DtxR (*8*, *16*, *20*). In the structures of Ni-DtxR(E9A,C102D) and Ni-DtxR(M10A,C102D), Oδ of Asp6 comes sufficiently close to the amide N of Glu9 to interact with the carbonyl oxygen of Leu4 as observed in the structure of Ni-DtxR-(D6A,C102D). As a result of the α-helical conformation observed for Leu4, Val5, and Asp6 in Ni-DtxR(D6A,-C102D), the carbonyl oxygen of Leu4 cannot mediate the interaction between a water molecule and the metal ion at binding site 2. Despite metal ion coordination in binding site 2, the backbone dihedral angles for Val5 are now in a traditionally allowed region for an α-helix. In the structure of Ni-DtxR(E9A,C102D), a hydrogen bond between Oγ of Glu9 and Nδ of His106 is lost as a result of the E9A mutation. His106 is a ligand for binding site 2. In addition to the loss of a protein ligand at binding site 2, replacement of Met10 with alanine in Ni-DtxR(M10A,C102D) results in a displacement of Cα by 0.6 Å compared to that of Ni-DtxR-(D6A,C102D). This rather small change affects the lengths of several backbone hydrogen bonds with neighboring residues.

Conformation of the Helix−Turn−Helix Motif. The HTH motif of DtxR is located in the N-terminal domain, is formed by helices B and C (residues 27−50), and is responsible for binding to the major groove of the operator DNA (*4*, *5*, *20*). This HTH motif is associated with DNA recognition and undergoes a conformational change upon DNA binding (*18*). A hydrogen bond network involving residues from the turn of the HTH motif (Gln36, Ser37, and Thr40) and the phosphate atoms of the DNA has been described (*21*). Furthermore, Pro39 and Ser37 participate as thymine-specific ligands in DNA binding (*21*). These interactions have also been found in the structural and functional DtxR homologue IdeR from *M. tuberculosis* (*19*). The HTH motifs of the DtxR mutants reported here do not show changes in conformation with respect to the active repressor. A hydrogen bonding network mediated by water molecules can also be observed in all the structures. Oγ of Thr40 shares a water molecule with Oγ of Ser37. A water molecule mediates the interaction

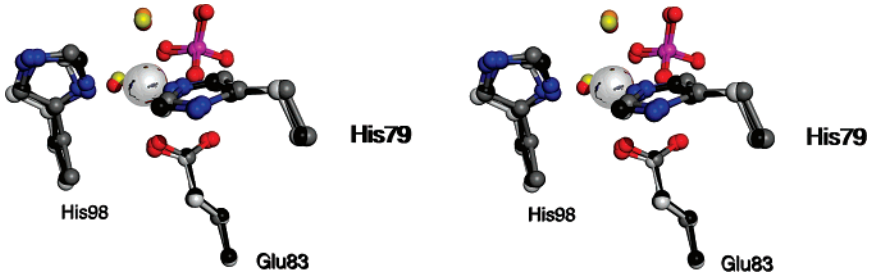

FIGURE 3: Stereoview of binding site 1 of Ni-DtxR(D6A,C102D), Ni-DtxR(E9A,C102D), and Ni-DtxR(M10A,C102D). The structures of Ni-DtxR(D6A,C102D) (dark gray), Ni-DtxR(E9A,C102D) (medium gray), and Ni-DtxR(M10A,C102D) (light gray) display almost identical positions for the protein ligands. A phosphate ion is present in all of the structures. In the structures of Ni-DtxR(D6A,C102D) and Ni-DtxR(E9A,C102D), there are two water molecules that complete the octahedral geometry, colored red and yellow, respectively. A single water molecule is found in the coordinating environment of binding site 1 of Ni-DtxR(E9A,C102D), colored orange. The distances from the ligands to the metal ions can be found in Table 2.

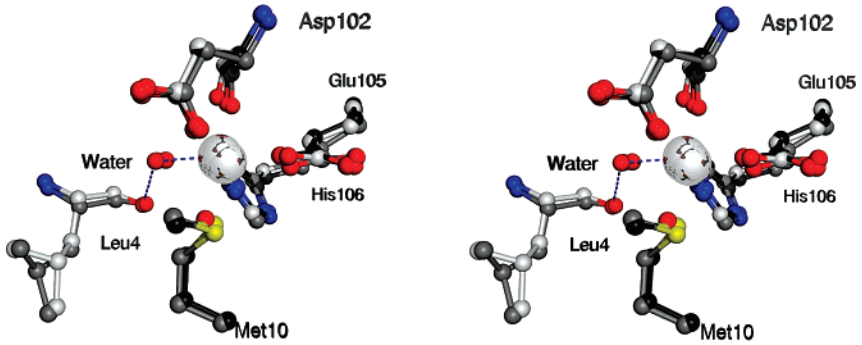

FIGURE 4: Stereoview of binding site 2 of Ni-DtxR(D6A,C102D), Ni-DtxR(E9A,C102D), and Ni-DtxR(M10A,C102D). The structures of Ni-DtxR(D6A,C102D) (dark gray), Ni-DtxR(E9A,C102D) (medium gray), and Ni-DtxR(M10A,C102D) (light gray) exhibit identical geometries. Both the structures of Ni-DtxR(E9A,C102D) and Ni-DtxR(M10A,C102D) show the water-mediated interaction with Leu4. A water molecule, colored red, replaces Met10 in Ni-DtxR(M10A,C102D). The distances from the ligands to the metal ions can be found in Table 3.

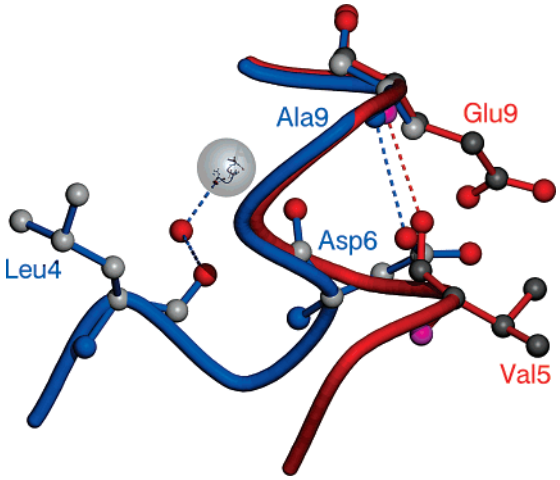

FIGURE 5: Comparison of the helical and nonhelical conformations of residues 3−10 corresponding to the N-terminal helix. The N-terminal helix of Ni-DtxR(D6A,C102D), colored red, displays the helical conformation observed in structures of the apo repressor. The NH groups of Ala6 and Glu9 are colored magenta for clarity. The N-terminal helix of Ni-DtxR(E9A,C102D), colored blue, shows the nonhelical conformation observed in the structures of the holo repressor. The structures of Ni-DtxR(M10A,C102D), Ni-DtxR(C102D), and DtxR(H79A,C102D) show identical nonhelical conformations (not shown for clarity). The structure of apo DtxR(H79A) can be superimposed with the helical conformation.

between Cδ of Gln43 and Oγ of Thr40. Also, Oγ of Ser42 interacts with the NH1 group of Arg27. Finally, the OH group from Tyr11 interacts with Oϵ of Gln36 via a water-mediated interaction.

Binding Affinities. Isothermal titration calorimetry was used to determine the relative binding affinities of DtxR(D6A,C102D), DtxR(E9A,C102D), and DtxR(M10A,C102D) for Ni(II) ion. The titrations of all the mutants used in this study best fitted a two-binding site model. A single-site model and a two-interacting sites model were also tried, but the resulting fits for the calorimetric titrations were not as good. These results are consistent with previous results obtained in our laboratory (*16*). Titrations performed using 1 mM Ni(II) ion show two distinct peaks consistent with a multistep binding model. Increasing the Ni(II) ion concentration to 3 mM leads to improvements in the fit. Figure 6 shows the titration of DtxR(D6A,C102D) with 3 mM Ni(II). Concentrations of metal ion of $\leq$10 mM were needed to saturate the low-affinity binding site in the titrations of DtxR(M10A,C102D). The calorimetric titrations of DtxR(E9A,C102D) and DtxR(M10A,C102D) exhibit traces similar to that of DtxR(D6A,C102D). The values of the relative binding affinities obtained in this study are shown in Table 4. The values of the binding affinities extracted from the titrations of the DtxR(D6A,C102D) and DtxR(E9A,C102D) mutants with Ni(II) ion are very similar to those obtained for the DtxR(C102D) mutant. However, as anticipated, the relative binding affinities of DtxR(M10A,C102D) for Ni(II) ion are different, particularly at the low-affinity binding site (see Table 4). Although the issue of cooperativity between the two binding sites was not specifically investigated in this study, the presence of a high-affinity and a low-affinity binding site does not seem consistent with a cooperative binding mechanism.

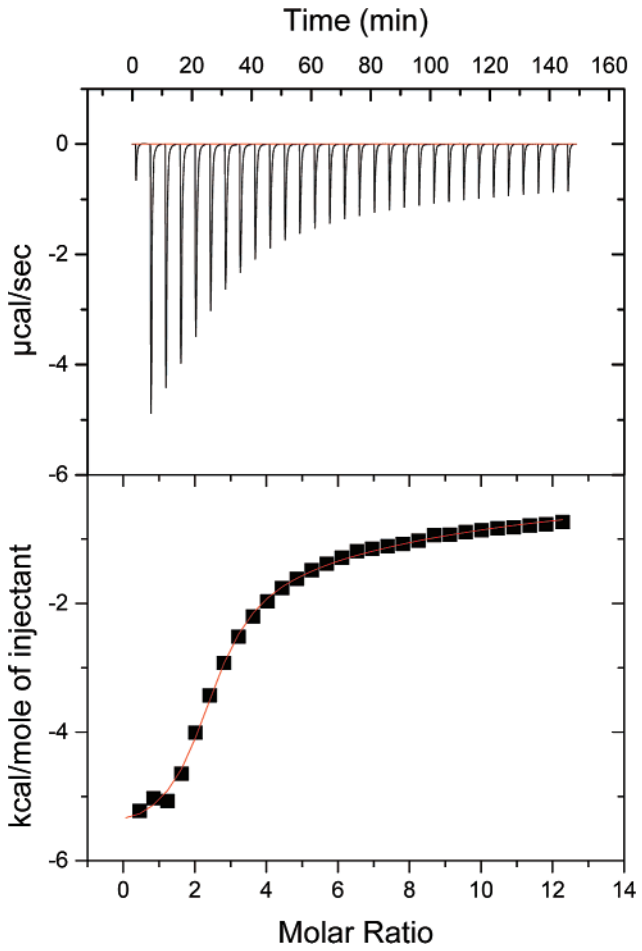

FIGURE 6: Calorimetric titration of DtxR(D6A,C102D) with $NiCl_2$. The top panel shows the actual heats associated with each injection of $NiCl_2$ (3 mM) to a total protein concentration of 55 μM. The bottom panel shows the fit to a two-binding site model. The binding affinities derived from calorimetric titrations are reported in Table 4.

Table 4: Metal Ion Binding Affinities for DtxR Mutants Presented in This Study

protein	high-affinity binding site[a]	low-affinity binding site[a]
DtxR(C102D)[b]	$(1.8 \pm 0.4) \times 10^{-7}$	$(1.6 \pm 0.3) \times 10^{-4}$
DtxR(D6A,C102D)	$(4.3 \pm 0.8) \times 10^{-6}$	$(4.0 \pm 0.6) \times 10^{-4}$
DtxR(E9A,C102D)	$(3.9 \pm 0.3) \times 10^{-7}$	$(1.1 \pm 0.5) \times 10^{-4}$
DtxR(M10A,C102D)	$(2.6 \pm 0.9) \times 10^{-6}$	$>1.1 \times 10^{-3}$

[a] The binding affinities were calculated using a 1 M standard state. [b] Values calculated from ref *16*.

DISCUSSION

The structures of Ni-DtxR(D6A,C102D), Ni-DtxR(E9A,-C102D), and Ni-DtxR(M10A,C102D) and the calorimetric measurement of relative binding affinities presented in this paper represent the first attempt to correlate structural data for N-terminal helix mutants with the metal ion-induced activation of DtxR-like repressors. The metal ion-induced activation of DtxR is characterized by conformational changes that can be monitored by crystallographic experiments. The extent of these changes in the crystallographic experiments highlights the delicate nature of the activation process in which DtxR acquires a persistent tertiary structure with minimal changes in secondary structure (*30*). These conformational changes are observed primarily in the N-terminal helix region.

In previously published structures of the activated form of DtxR, where the dimer is formed noncrystallographically, the HTH motif of the second subunit is displaced (*5*, *18*, *20*). This conformational change, observed only in the metal ion-bound form of DtxR, was attributed to metal ion-induced activation. Because all the mutants studied here crystallize in space group $P3_121$, which contains only one molecule in the asymmetric unit, the dimer is formed crystallographically. Consequently, possible domain motion between subunits could not be observed in these structures. However, the N-terminal domains of all the mutants studied here display a conformation around the turn of the HTH motif identical to that observed in the crystal structure of the Ni-DtxR-(C102D)−DNA complex (*20*). Because Ni-DtxR(D6A,-C102D), Ni-DtxR(E9A,C102D), and Ni-DtxR(M10A,-C102D) all show both metal ion binding sites occupied, it is reasonable that their HTH motifs adopt the active conformation. The HTH motifs of Ni-DtxR(D6A,C102D), Ni-DtxR(E9A,C102D), and Ni-DtxR(M10A,C102D) are stabilized by four water-mediated interactions with side chains. One of these water-mediated interactions involves Oϵ of Gln36 and the OH group from Tyr11, which is adjacent to Met10, a binding site 2 ligand. It is therefore possible that metal ion coordination at site 2 influences the conformation of the HTH motif in the activated form of the repressor by modulating the strength of this water-mediated interaction.

Without a conformational change, the N-terminal helix of DtxR would have an unfavorable steric interaction with the DNA, and this could result in a loss of repressor activity (*5*). A nonhelical conformation of the first six residues of the N-terminal helix is observed upon metal ion-induced activation (*20*). This conformational change is accompanied by a water-mediated interaction between the metal ion and the carbonyl oxygen of Leu4 that places the backbone dihedral angles of Val5 outside the energetically favored regions for an α-helix (*20*). It has been suggested that the existence of such conformations may lead to stabilization of the structure (*31*). The water-mediated interaction was also observed in the activated form of IdeR (*29*). The occurrence of this interaction in several structures of both DtxR and IdeR suggests that it plays an important role in the repressor activity of DtxR-like repressors. The high degree of conservation at the primary sequence level of the N-terminal helix of DtxR-like repressors seems to support this hypothesis. In fact, a BLAST search using the first 21 residues of the sequence of DtxR yields more than 35 sequences that are more than 80% identical (17 of 21), all annotated as DtxR-like proteins and mostly from Gram-positive bacteria. These putative DtxR homologues cover a wide variety of bacterial organisms. From the functional point of view, the activity of DtxR(D6A) and DtxR(E9A) is decreased with respect to that of wild-type DtxR (*8*). Since these mutations are located in the N-terminal helix but do not involve residues that participate in metal ion binding in either binding site, the decreased activity exhibited by these mutants must be related to the conformational change associated with metal ion-induced activation of DtxR. Because previously published structures of DtxR complexed with a variety of divalent transition metal ions show no correlation between the conformation of the protein and the nature of the cation, and

because the choice of complexing cation does not affect the geometry and the coordination number in those structures, the observed conformational changes in these N-terminal mutants are not likely due to the use of Ni(II) for Fe(II), which is the physiological cation in vivo (*4*, *11*). In addition, the conformation of this region may affect the ability of DtxR to dimerize. In fact, the mutant gsh-DtxR(C102D), which contains a Gly-Ser-His extension at the N-terminus, has a different conformation in the N-terminal region and is unable to dimerize (*30*).

The shape of the calorimetric titrations of DtxR(D6A,-C102D), DtxR(E9A,C102D), and DtxR(M10A,C102D) suggests that there are no differences in the binding scheme of these or other previously studied DtxR mutants. Because metal ion reconstitution experiments have established that DtxR has approximately the same binding affinity for Fe(II) and Ni(II), we have used a nonphysiological cation, Ni(II), in the titrations described here. This choice has enabled us to compare these new results to previous data. The relative binding affinities for metal ion obtained for these mutants are consistent with our previous measurements for the wild type and other DtxR mutants (*16*). The fact that binding site 2 in Ni-DtxR(M10A,C102D) is fully occupied despite the M10A mutation indicates that metal ion binding at that site is still possible, albeit with a lower binding affinity. The results indicate that the probability of coordinating metal ion in a mutated binding site 2 is still higher than in any other region of the protein and could be overcome by increasing the ligand concentration. Only in the structure of DtxR(H79A), whose binding site 2 is blocked due to derivatization of Cys102, have we detected a complete loss of metal ion in binding site 2, and as a result, this mutant does not show signs of metal ion-induced activation in vitro (*16*).

The first six N-terminal residues of Ni-DtxR(M10A,-C102D) are in the nonhelical conformation characteristic of the activated form of DtxR-like repressors despite the decrease in the binding affinity of binding site 2. However, DtxR(M10A) is not an active repressor in vivo. It is therefore likely that the loss of repressor activity in DtxR(M10A) is due to a decreased binding affinity at binding site 2 as a result of the M10A mutation rather than by an altered conformation of the binding site triggered by replacement of either Glu9 or Asp6 as a ligand as previously suggested (*32*). The high degree of conservation of Met10 among DtxR-like repressors is indicative of its importance in repressor activity. These results suggest that Met10 provides the linkage between metal ion binding and the conformation of the N-terminal helix.

The structure of Ni-DtxR(E9A,C102D) also shows an active conformation, and the binding affinities for metal ion are very similar to those obtained for DtxR(C102D). Glu9 participates in a salt bridge with His106, which is directly involved in metal ion binding. This interaction is observed in all structures reported in this paper, and also that of apo DtxR(H79A). This interaction is absent in Ni-DtxR(E9A,-C102D) as a result of the Ala replacement. For this reason, we believe that the lower repressor activity of DtxR(E9A) is connected with the loss of this interaction. The higher *B*-factor (which may be connected with a lower occupancy) observed for Ni(II) ion at binding site 2 would suggest that the metal ion is less tightly bound. However, we were not able to detect significant changes in binding affinity resulting from such a loss. A possible explanation is that the observed decrease in activity resulting from the loss of a hydrogen bond does not lead to significant changes in binding affinity.

The DtxR(D6A,C102D) mutant has some unusual properties. On the one hand, this mutant coordinates metal ion in both binding sites, and on the other, the N-terminal helix of Ni-DtxR(D6A,C102D) remains helical after metal ion binding at site 2. DtxR(D6A) is active in vivo, albeit with reduced activity. The D6A mutation alters the energetic balance of the N-terminal region of the protein and increases the probability of the persistence of the helical conformation. Ni-DtxR(D6A,C102D) has allowed us to separate the effect of metal ion binding from conformational changes that take place in the N-terminal helix upon activation. In structures of DtxR not bearing the D6A mutation, after coordination at site 2, a hydrogen bond that arises from the interaction between the carbonyl oxygen of Leu4 and the water molecule coordinated to the metal ion stabilizes the nonhelical conformation. This interaction is energetically favorable. Additional stabilization comes from the replacement of Oδ1 of Asp6 with the carbonyl oxygen of Val5 in a hydrogen bond with the main chain nitrogen of Glu9, as the conformational change takes place. This interaction prevents unfolding of an additional helical turn. It is for this reason that the backbone dihedral angles found for Val5 are outside energetically favorable regions in the nonhelical conformation. The D6A mutation prevents this interaction as the side chain of Ala is not able to participate in hydrogen bonding. As a result, Ni-DtxR(D6A,C102D) is unable to sustain the water-mediated interaction between the metal ion coordinated to binding site 2 and the carbonyl oxygen of Leu4, and the helical conformation is observed. The presence of an additional Ala in the N-terminal helix also contributes to stabilization of this region of the protein. The stabilization of the backbone of proteins by Ala is well-understood (*33*−*37*). These changes can account for the decrease in repressor activity observed in DtxR(D6A). Interestingly, binding site 1 of both Ni-DtxR(D6A,C102D) and DtxR(E9A,C102D) displays octahedral geometry, which has never been seen before in DtxR or its mutants. It is possible that the expansion of the coordination sphere of binding site 1 of these two mutants could be related to the perturbation of the N-terminal helix induced by the D6A and E9A mutations. In the structure of DtxR(H79A), which has an intact Asp6 and no metal ion coordination at site 2, Oδ1 of Asp6 hydrogen bonds with N of Asp3 and Nζ of Lys2 and interacts with the carbonyl oxygen of Arg103. It is possible that the loss of these interactions is responsible for the flexibility of the first two residues in Ni-DtxR(D6A,C102D). In a recently published structure of the IdeR−DNA complex, the equivalent residue, Asn2, is located 3.8 Å from a phosphate oxygen of DNA (*19*).

With the exception of Ni-DtxR(D6A,C102D), all activated structures of DtxR and its mutants, even those that have reduced activity, show the N-terminal helix in an identical conformation. Our results show that this conformation is not arbitrary. In addition, because an identical conformation has been identified in both DtxR and IdeR, we also believe that this interaction could be general to DtxR-like repressors. So in essence, the conformational change observed in the N-terminal region of DtxR cannot be regarded simply as a

helix-to-coil transition in the sense that the coil conformation is not random.

Our results explain the decrease in activity of N-terminal helix mutants first observed by Ding et al. at a molecular level and have improved our understanding of the process of metal ion-induced activation of DtxR (*8*). We have mapped the interactions that determine the conformational change of the N-terminal helix upon metal ion-induced activation. We have also shown the effect that several mutations in this region of the protein have on its conformation. These changes occur without significant changes in binding affinities. Our results demonstrate that the N-terminal helix plays an important role in the metal ion-induced activation of DtxR by acting as a very subtle but effective sensor of activating metal ions and triggering a critical conformational change that enables the repressor to recognize DNA. The combination of metal ion binding that provides a persistent three-dimensional structure and the conformational change observed in the N-terminal helix, which relieves potentially unfavorable steric interaction with the DNA, accounts for most of the regulatory properties of DtxR. In addition, the side chain of Asp6 seems to be required for stabilization of the nonhelical conformation by a helical capping interaction (*38*, *39*).

ACKNOWLEDGMENT

We are grateful to the Biophysical Instrumentation Facility for the Study of Complex Macromolecular Systems at the Massachusetts Institute of Technology (National Science Foundation Grant NSF-0070319 and NIH Grant GM68762) for calorimetric measurements. GM/CA CAT has been funded in whole or in part with federal funds from the National Cancer Institute (Y1-CO-1020) and the National Institute of General Medical Sciences (Y1-GM-1104). Use of the Advanced Photon Source was supported by the U.S. Department of Energy, Basic Energy Sciences, Office of Science, under Contract W-31-109-ENG-38. We are grateful to Dr. Chris Miller for the use of the X-ray generator.

REFERENCES

1. Schmitt, M. P., Predich, M., Doukhan, L., Smith, I., and Holmes, R. K. (1995) Characterization of an iron-dependent regulatory protein (IdeR) of *Mycobacterium tuberculosis* as a functional homolog of the diphtheria toxin repressor (DtxR) from *Corynebacterium diphtheriae*, *Infect. Immun. 63*, 4284−4289.
2. Bates, C. S., Toukoki, C., Neely, M. N., and Eichenbaum, Z. (2005) Characterization of MtsR, a new metal regulator in group A *Streptococcus*, involved in iron acquisition and virulence, *Infect. Immun. 73*, 5743−5753.
3. Posey, J. E., Hardham, J. M., Norris, S. J., and Gherardini, F. C. (1999) Characterization of a manganese-dependent regulatory protein, TroR, from *Treponema pallidum*, *Proc. Natl. Acad. Sci. U.S.A. 96*, 10887−10892.
4. Qiu, X., Verlinde, C. L., Zhang, S., Schmitt, M. P., Holmes, R. K., and Hol, W. G. (1995) Three-dimensional structure of the diphtheria toxin repressor in complex with divalent cation corepressors, *Structure 3*, 87−100.
5. Schiering, N., Tao, X., Zeng, H., Murphy, J. R., Petsko, G. A., and Ringe, D. (1995) Structures of the apo- and the metal ion-activated forms of the diphtheria tox repressor from *Corynebacterium diphtheriae*, *Proc. Natl. Acad. Sci. U.S.A. 92*, 9843−9850.
6. Glasfeld, A., Guedon, E., Helmann, J. D., and Brennan, R. G. (2003) Structure of the manganese-bound manganese transport regulator of *Bacillus subtilis*, *Nat. Struct. Biol. 10*, 652−657.
7. Que, Q., and Helmann, J. D. (2000) Manganese homeostasis in *Bacillus subtilis* is regulated by MntR, a bifunctional regulator related to the diphtheria toxin repressor family of proteins, *Mol. Microbiol. 35*, 1454−1468.
8. Ding, X., Zeng, H., Schiering, N., Ringe, D., and Murphy, J. R. (1996) Identification of the primary metal ion-activation sites of the diphtheria, tox repressor by X-ray crystallography and site-directed mutational analysis, *Nat. Struct. Biol. 3*, 382−387.
9. Pohl, E., Holmes, R. K., and Hol, W. G. (1999) Crystal structure of a cobalt-activated diphtheria toxin repressor-DNA complex reveals a metal-binding SH3-like domain, *J. Mol. Biol. 292*, 653−667.
10. Pohl, E., Qui, X., Must, L. M., Holmes, R. K., and Hol, W. G. (1997) Comparison of high-resolution structures of the diphtheria toxin repressor in complex with cobalt and zinc at the cation-anion binding site, *Protein Sci. 6*, 1114−1118.
11. Qiu, X., Pohl, E., Holmes, R. K., and Hol, W. G. (1996) High-resolution structure of the diphtheria toxin repressor complexed with cobalt and manganese reveals an SH3-like third domain and suggests a possible role of phosphate as co-corepressor, *Biochemistry 35*, 12292−12302.
12. Diller, D. J., Redinbo, M. R., Pohl, E., and Hol, W. G. (1999) A database method for automated map interpretation in protein crystallography, *Proteins 36*, 526−541.
13. Goranson-Siekierke, J., Pohl, E., Hol, W. G., and Holmes, R. K. (1999) Anion-coordinating residues at binding site 1 are essential for the biological activity of the diphtheria toxin repressor, *Infect. Immun. 67*, 1806−1811.
14. Spiering, M. M., Ringe, D., Murphy, J. R., and Marletta, M. A. (2003) Metal stoichiometry and functional studies of the diphtheria toxin repressor, *Proc. Natl. Acad. Sci. U.S.A. 100*, 3808−3813.
15. Tao, X., and Murphy, J. R. (1992) Binding of the metalloregulatory protein DtxR to the diphtheria tox operator requires a divalent heavy metal ion and protects the palindromic sequence from DNase I digestion, *J. Biol. Chem. 267*, 21761−21764.
16. D'Aquino, J. A., Tetenbaum-Novatt, J., White, A., Berkovitch, F., and Ringe, D. (2005) Mechanism of metal ion activation of the diphtheria toxin repressor DtxR, *Proc. Natl. Acad. Sci. U.S.A. 102*, 18408−18413.
17. Golynskiy, M. V., Gunderson, W. A., Hendrich, M. P., and Cohen, S. M. (2006) Metal Binding Studies and EPR Spectroscopy of the Manganese Transport Regulator MntR, *Biochemistry 45*, 15359−15372.
18. Pohl, E., Holmes, R. K., and Hol, W. G. (1998) Motion of the DNA-binding domain with respect to the core of the diphtheria toxin repressor (DtxR) revealed in the crystal structures of apo- and holo-DtxR, *J. Biol. Chem. 273*, 22420−22427.
19. Wisedchaisri, G., Holmes, R. K., and Hol, W. G. (2004) Crystal structure of an IdeR-DNA complex reveals a conformational change in activated IdeR for base-specific interactions, *J. Mol. Biol. 342*, 1155−1169.
20. White, A., Ding, X., vanderSpek, J. C., Murphy, J. R., and Ringe, D. (1998) Structure of the metal-ion-activated diphtheria toxin repressor/tox operator complex, *Nature 394*, 502−506.
21. Chen, C. S., White, A., Love, J., Murphy, J. R., and Ringe, D. (2000) Methyl groups of thymine bases are important for nucleic acid recognition by DtxR, *Biochemistry 39*, 10397−10407.
22. Collaborative Computational Project Number 4 (1994) The CCP4 suite: Programs for protein crystallography, *Acta Crystallogr. D50*, 760−763.
23. Leslie, A. G. W. (1992) *Joint CCP4 + ESF-EAMCB Newsletter on Protein Crystallography*, Vol. 26, UK:SERC Daresbury Laboratory, Warrington, U.K.
24. Otwinowski, Z., and Minor, W. (1997) Processing of X-ray diffraction data collected in oscillation mode, Methods in Enzymology, Volume 276: *Macromolecular Crystallography, Part A*, (Carter, C. W., Jr., Sweet, R. M., Eds.) pp 307−326, Academic Press, New York.
25. Murshudov, G. N., Vagin, A. A., and Dodson, E. J. (1997) Refinement of macromolecular structures by the maximum-likelihood method, *Acta Crystallogr. D53*, 240−255.
26. D'Aquino, J. A., and Ringe, D. (2003) Determinants of the Src homology domain 3-like fold, *J. Bacteriol. 185*, 4081−4086.
27. Ramachandran, G. N., Ramakrishnan, C., and Sasisekharan, V. (1963) Stereochemistry of Polypeptide Chain Configurations, *J. Mol. Biol. 7*, 95.
28. Pohl, E., Holmes, R. K., and Hol, W. G. (1999) Crystal structure of the iron-dependent regulator (IdeR) from *Mycobacterium tuberculosis* shows both metal binding sites fully occupied, *J. Mol. Biol. 285*, 1145−1156.

29. Feese, M. D., Ingason, B. P., Goranson-Siekierke, J., Holmes, R. K., and Hol, W. G. (2001) Crystal structure of the iron-dependent regulator from *Mycobacterium tuberculosis* at 2.0-Å resolution reveals the Src homology domain 3-like fold and metal binding function of the third domain, *J. Biol. Chem. 276*, 5959−5966.
30. Twigg, P. D., Parthasarathy, G., Guerrero, L., Logan, T. M., and Caspar, D. L. (2001) Disordered to ordered folding in the regulation of diphtheria toxin repressor activity, *Proc. Natl. Acad. Sci. U.S.A. 98*, 11259−11264.
31. McCaldon, P., and Argos, P. (1988) Oligopeptide Biases in Protein Sequences and Their Use in Predicting Protein Coding Regions in Nucleotide Sequences, *Proteins 4*, 99−122.
32. Rangachari, V., Marin, V., Bienkiewicz, E. A., Semavina, M., Guerrero, L., Love, J. F., Murphy, J. R., and Logan, T. M. (2005) Sequence of ligand binding and structure change in the diphtheria toxin repressor upon activation by divalent transition metals, *Biochemistry 44*, 5672−5682.
33. Padmanabhan, S., Marqusee, S., Ridgeway, T., Laue, T. M., and Baldwin, R. L. (1990) Relative helix-forming tendencies of nonpolar amino acids, *Nature 344*, 268−270.
34. Creamer, T. P., and Rose, G. D. (1994) α-Helix-forming propensities in peptides and proteins, *Proteins 19*, 85−97.
35. O'Neil, K. T., and DeGrado, W. F. (1990) A thermodynamic scale for the helix-forming tendencies of the commonly occurring amino acids, *Science 250*, 646−651.
36. Lyu, P. C., Liff, M. I., Marky, L. A., and Kallenbach, N. R. (1990) Side chain contributions to the stability of α-helical structure in peptides, *Science 250*, 669−673.
37. D'Aquino, J. A., Gomez, J., Hilser, V. J., Lee, K. H., Amzel, L. M., and Freire, E. (1996) The magnitude of the backbone conformational entropy change in protein folding, *Proteins 25*, 143−156.
38. Serrano, L., and Fersht, A. R. (1989) Capping and α-helix stability, *Nature 342*, 296−299.
39. Richardson, J. S., and Richardson, D. C. (1988) Helix lap-joints as ion-binding sites: DNA-binding motifs and Ca-binding "EF hands" are related by charge and sequence reversal, *Proteins 4*, 229−239.
40. Fenn, T. D., Ringe, D., and Petsko, G. A. (2003) POVScript+: A program for model and data visualization using persistence of vision ray-tracing, *J. Appl. Crystallogr. 36*, 944−947.
41. Kraulis, P. J. (1991) Molscript: A Program to Produce Both Detailed and Schematic Plots of Protein Structures, *J. Appl. Crystallogr. 24*, 946−950.

BI7007883